Journal of Inflammation Research

Dovepress
Taylor & Francis Group

Open Access Full Text Article

ORIGINAL RESEARCH

Dose-Weighted Network Pharmacology: Evaluating Traditional Chinese Medicine Formulations for Lumbar Disc Herniation

Changwen Zhou[1], Ting Xiang[2], Yu Yu[3], Hongzhong Ma[1], Ce Liu[1], Feng Yang[1,4,*], Lixue Yang[1,4,*]

[1]The First Clinical Medical College, Shaanxi University of Chinese Medicine, Shaanxi, People's Republic of China; [2]Rehabilitation Department, Xiang Xi Autonomous Prefecture National Hospital, Hunan, People's Republic of China; [3]Department of Chinese Medicine, Minda Hospital of Hubei Minzu University, Hubei, People's Republic of China; [4]Department of Orthopedic Hospital, The Affiliated Hospital of Shaanxi University of Chinese Medicine, Shaanxi, People's Republic of China

*These authors contributed equally to this work

Correspondence: Lixue Yang; Feng Yang, The First Clinical Medical College, Shaanxi University of Chinese Medicine, Vice No. 2, West Weiyang Road, Qindu District, Shaanxi, 712000, People's Republic of China, Email ylx18391076233@163.com; yangfengdudu@163.com

Background and Purpose: Lumbar disc herniation (LDH) significantly impacts individuals, particularly those aged 40–45. Traditional Chinese Medicine (TCM) formulations such as Taohong Siwu Decoction (TSD), Yaotong Jizheng Decoction (YJD), and Panlong Qi Tablet (PQT) are widely used for treatment. This study introduces dose-weighted network pharmacology, a novel approach that incorporates drug dosage as a quantitative factor into network analysis to evaluate better and compare the therapeutic potential of TCM formulations.

Methods: This study combines drug dosage with the PPI network to propose a theoretical algorithm for comparing the therapeutic efficacy of different traditional Chinese medicine formulations. The VIKOR method was used to assess the importance of therapeutic targets, with weights assigned based on both drug and disease perspectives. TSD, YJD, and PQT were evaluated in animal experiments, and the algorithm's feasibility was validated through GO and KEGG pathway analysis, Thermal Hyperalgesia Test, H&E staining, Western blotting (WB), RT-PCR, and ELISA assays.

Results: The computational model indicated that YJD and PQT had higher predicted efficacy compared to TSD. These predictions were confirmed in animal studies, where YJD demonstrated the greatest reduction in thermal hyperalgesia and the most significant decrease in inflammatory markers, surpassing both TSD and PQT. GO and KEGG pathway analyses highlighted key pathways related to oxidative stress and inflammation, providing mechanistic insights into the effectiveness of the treatments.

Conclusion: Incorporating dosage as a reference factor into network pharmacology research proved feasible and effective, emphasizing the importance of precise dosage control in TCM formulations for treating LDH. The new algorithm provided reliable predictions, demonstrating its potential to enhance the design and evaluation of TCM formulations. Future improvements, such as establishing a target acceptance rate database, could further refine the algorithm, expanding its application in personalized medicine and targeted therapy.

Keywords: dose-weighted network pharmacology, lumbar disc herniation, traditional Chinese medicine, Panlong Qi Tablet, Taohong Siwu decoction, VIKOR

Introduction

In the literature indexed by the Web of Science Core Collection, Albeck[1] was the first to use the term "Lumbar Disc Herniation" (LDH) to describe the protrusion of disc contents caused by the rupture of the annulus fibrosus. Over the past thirty years since the publication of this work, epidemiological reports have indicated that LDH affects the daily lives of approximately 9% of the global population, with the incidence increasing in tandem with population aging.[2]

Given the lower back pain and economic burden associated with LDH, extensive research has focused on treatment strategies. Studies on patient adherence suggest that addressing lower limb pain can significantly improve treatment

Received: 11 October 2024
Accepted: 18 January 2025
Published: 27 January 2025

compliance.[3] While surgical interventions may yield superior outcomes, non-surgical treatments remain the preferred choice for most newly diagnosed LDH patients.[2,4] Among non-surgical options, traditional Chinese medicine (TCM) has shown unique strength.[5]

The unique strength of TCM lies in its flexibility to adapt formulations based on specific conditions.[6] The advent of network pharmacology has facilitated a more intuitive understanding of the molecular mechanisms underlying TCM, addressing prior uncertainties.[7] By employing complex network models, network pharmacology enables a systematic evaluation of TCM efficacy, and its approach has gained substantial recognition.[8] However, challenges remain in simplifying TCM formulations within these models. In particular, the omission of dosage considerations leads to overly idealized assumptions, such as different doses producing the same levels of active ingredients, which could skew predictions of therapeutic outcomes. Despite these limitations, the "drug-active ingredient-target-disease" pathways have validated the potential for data transmission, and with appropriate computational models, drug dosage information could be incorporated into network analyses.

Accordingly, this study included Taohong Siwu Decoction (TSD) and a modified version of TSD for LDH, known as Yaotong Jizheng Decoction (YJD), developed by Professor Yang Lixue, a renowned TCM practitioner from Shaanxi Province. These were compared with the commonly used Chinese patent medicine Panlong Qi Tablet (PQT). Utilizing the Vlsekriterijumska Optimizacija I Kompromisno Resenje (VIKOR)[9] scoring method, we developed a TCM formula efficacy scoring algorithm based on the protein–protein interaction (PPI) network and drug dosage. This study aims to explore the feasibility of incorporating dosage factors into TCM omics analysis. The complete research process is illustrated in Figure 1.

Materials and Methods

Drug Quantification and Target Collection

The 6 drugs in TSD use doses recorded in the Qianlong 7th Year Wuying Palace printed edition. The 9 drugs in YJD use common clinical doses. The 29 drugs in PQT (National Medicine Standard Z61020050) use doses according to the national standards.

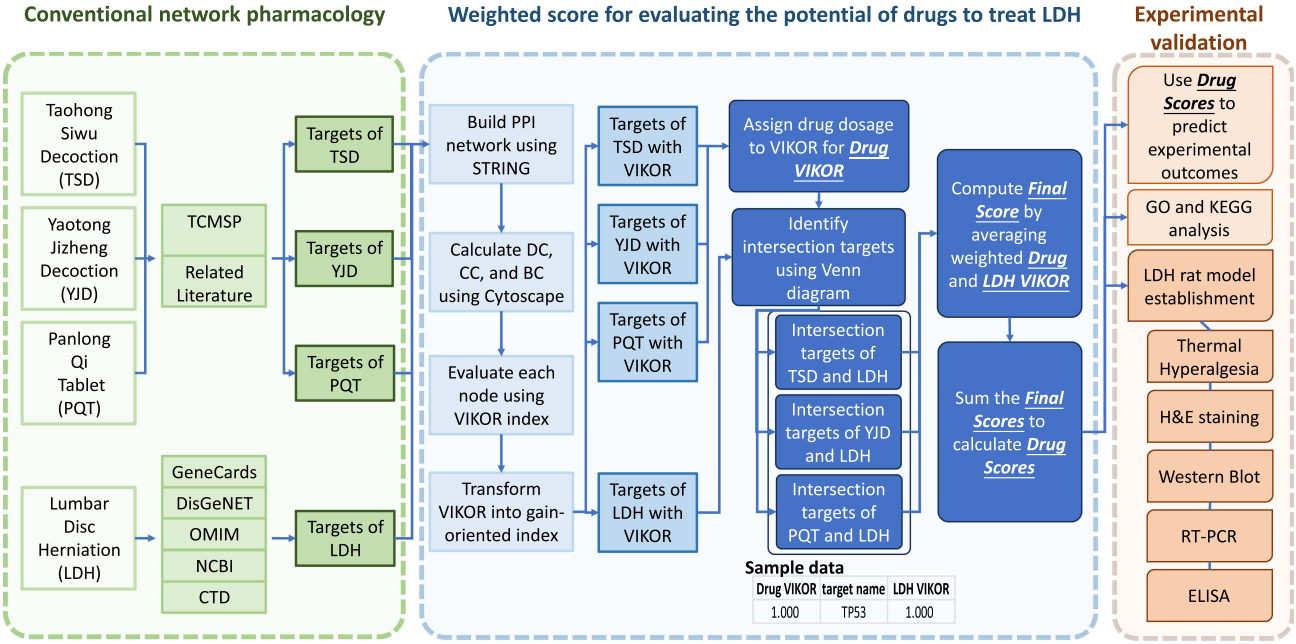

Figure 1 Technical roadmap for weighted network scoring and experimental validation.
Abbreviations: DC, Degree Centrality; CC, Closeness Centrality; BC, Betweenness Centrality; GO, Gene Ontology; KEGG, Kyoto Encyclopedia of Genes and Genomes; VIKOR, Vlsekriterijumska Optimizacija I Kompromisno Resenje; Drug VIKOR, VIKOR parameters in terms of drug; Final Score, The final target parameter after mixing the two parameters (Drug VIKOR & LDH VIKOR); LDH VIKOR, VIKOR parameters in terms of Lumbar disc herniation; Drug Scores, The total number of scores for the targets contained in the drug.

After completing data entry, traditional network pharmacology methods are applied, using oral bioavailability (OB) ≥30% and drug-likeness (DL) ≥0.18 as screening criteria. Active ingredients of each drug are searched in the TCMSP database.[10] For drugs not included in the TCMSP database, relevant studies[11–13] are used to supplement the data. The chemical names, molecular formulas, and Canonical SMILES of each active ingredient are collected from the PubChem database[14]. Subsequently, the Canonical SMILES are input into the SwissTargetPrediction[15] database to identify the corresponding targets of the active ingredients.

Collection of LDH Targets

LDH-related targets were retrieved from the GeneCards,[16] DisGeNET,[17] OMIM,[18] NCBI[19] and CTD[20] databases using the search term "Lumbar Disc Herniation". The obtained targets were then organized, and duplicates were removed.

Discovery of Core Targets Based on PPI Network

Previous studies suggest that constructing a PPI network using the intersection of drug and disease targets can reveal the differential importance of drug action targets on diseases[21,22]. This study advances conventional network pharmacology by applying an extremization approach to construct the PPI network for three drugs and the disease. This approach hypothesizes a disease that perfectly matches all drug action targets, allowing each target to exert its effect, thus highlighting the importance of each drug target. Conversely, it also hypothesizes a drug whose targets perfectly match all pathogenic targets of LDH, enabling "treatment" of each target and highlighting their importance in treating LDH.

Based on these hypotheses, the targets of the three TCM formulas collected in Drug Quantification and Target Collection and the LDH targets collected in Collection of LDH Targets were input into the STRING[23] database for PPI network construction. The resulting networks were imported into Cytoscape software, where network topology parameters, including BC, DC, and CC, were analyzed using the Centiscape tool.

Comprehensive Target Scoring Algorithm VIKOR

Given the complexity of the network, using a single indicator to describe the importance of targets would be inadequate.[24] To overcome the limitations of a single indicator, this study employs a target importance ranking method based on multi-criteria decision-making (MCDM) — the VIKOR index.[9]

Matrix Construction

Given the undirected PPI network $D = (V)$ after calculating topological parameters using Centiscape, where V represents the set of all target nodes, $V = \{v_1, v_2, \ldots, v_n\}$, with the total number of targets denoted as $|V| = n$, and the set of target evaluation criteria (tec) is represented as $C = \{c_1, c_2, \ldots, c_m\}$, with a total of $|C| = m$ criteria. The matrix can be formulated as follows:

$$\boldsymbol{D} = \begin{bmatrix} v_1(c_1) & v_1(c_2) & \cdots & v_1(c_m) \\ v_2(c_1) & v_2(c_2) & \cdots & v_2(c_m) \\ \vdots & \vdots & \ddots & \vdots \\ v_n(c_1) & v_n(c_2) & \cdots & v_n(c_m) \end{bmatrix}$$

Here, $v_i(c_j)$ represents the value of the i−th target for the j−th criterion. In this study, the evaluation criteria are defined as $C = \{BC, DC, CC\}$.

Matrix Normalization

To eliminate dimensional differences between the criteria, the matrix D is normalized as:

$$r_{ij} = v_i(c_j) / \sum_{i=1}^{n} v_i(c_j)$$

In this formula, the numerator and denominator are fixed for each j, indicating the normalization of the data for criterion j. Once all criteria are normalized, the resulting normalized matrix is denoted as $R = (r_{ij})_{n \times m}$.

Assigning Weights to Criteria

For this study, all evaluation criteria are considered equally important, so the weight assigned to each criterion is $w_{tec} = 1/m$.

Ideal and Negative-Ideal Solutions

The ideal solution r_j^* and the negative solution r_j^- are defined as:

$$r_j^* = \left\{ (\max_i r_{ij} | j \in J) or (\min_i r_{ij} | j \in J') \right\}$$

$$r_j^- = \left\{ (\min_i r_{ij} | j \in J) or (\max_i r_{ij} | j \in J') \right\}$$

Here, J represents the set of benefit-type criteria, where higher values indicate greater importance of the target, and J'represents the set of cost-type criteria, where higher values are less favorable. In this study, all three criteria belong to the benefit-type.

Utility Measure and Regret Measure

The utility measure S_i and the regret measure R_i for all targets are computed as:

$$S_i = \sum_{j=1}^{m} w_j \left(r_j^* - r_{ij} \right) / \left(r_j^* - r_j^- \right)$$

$$R_i = \max_j \left[w_j \left(r_j^* - r_{ij} \right) / \left(r_j^* - r_j^- \right) \right]$$

VIKOR Index Calculation

The importance of each target is quantified using the VIKOR index, calculated as:

$$Q_i = v(S_i - S^*)/(S^- - S^*) + (1 - v)(R_i - R^*)/(R^- - R^*)$$

Where $S^* = min_i S_i$, $S^- = max_i S_i$, $R^* = min_i R_i$, $R^- = max_i R_i$. Here, v is the weight for the strategy of maximizing group utility, and $1 - v$ is the weight for individual regret, with $v = 0.5$.

VIKOR Index Transformation

Since the VIKOR index is a cost-type criterion and $Q_i \in [0, 1]$, Q_i is transformed to facilitate subsequent calculations:

$$Q_i^* = 1 - Q_i$$

Bilateral Target Weight

Frequency Conversion of Drug Dosage and Active Ingredient Production

Since the current research cannot accurately obtain the specific relationship between drugs and the output of their active ingredients, this study simplifies the issue by assuming that each gram of a drug corresponds to one production run of the active ingredient. Therefore, for "a" different drugs producing the same active ingredient A, we calculate:

$$AI_A^{Number\ of\ production\ runs} = \sum_{x=1}^{a} H_x^M$$

Where H_x^M represents the mass of drug x in grams.

Frequency of Active Ingredient Production and Target Interaction

Similarly, for "b" active ingredients acting on the same target B, the cumulative effect on the target is expressed as:

$$T_B^{nopr} = \sum_{y=1}^{b} AI_y^{nopr}$$

where T_B^{nopr} is the number of times target B is affected, and AI_y^{nopr} represents the number of production runs of active ingredient y. In this study, we assume that the more frequently a target is affected, the more frequently the biological processes associated with that target are triggered after binding.

Drug-Specific Weight Settings

By combining the formulas from Frequency Conversion of Drug Dosage and Active Ingredient Production and Frequency of Active Ingredient Production and Target Interaction, we can establish a logical pathway linking drug production of active ingredients to target influence, as depicted in Figure 2.

The value T_i^{nopr} represents the number of times target i is affected. A higher T_i^{nopr} indicates a stronger impact of the drug on target i. After normalization, this is converted into a drug-specific weight:

$$w_{i,D} = \left(\frac{T_i^{nopr} - T_{min}^{nopr}}{T_{max}^{nopr} - T_{min}^{nopr}} \right)$$

Disease-Specific Weight

As shown in the logical pathway in Figure 2, the disease-specific influence on the target does not follow the hierarchical structure observed on the drug side. The weight for the disease side is derived from the VIKOR score for LDH targets $Q_{i,L}^*$, which reflects the variability in the target's role in "treating" LDH, often due to individual differences. In this study, it is assumed that:

$$w_{i,L} = 1$$

Drug Scoring Calculation Method

Bilateral Target Weight Scoring

For each LDH target, the weight is calculated as follows:

$$LDH\ VIKOR_i = w_{i,L} \times Q_{i,L}^*$$

For each drug target, the corresponding weight is calculated as:

$$Drug\ VIKOR_i = w_{i,D} \times Q_{i,D}^*$$

Normalization of Drug-Specific Scores

Since the introduction of drug-specific weights in Bilateral Target Weight Scoring results in $DrugVIKOR_i$ having a range outside $[0, 1]$, a normalization step is performed to bring $DrugVIKOR_i$ in line with $LDHVIKOR_i$:

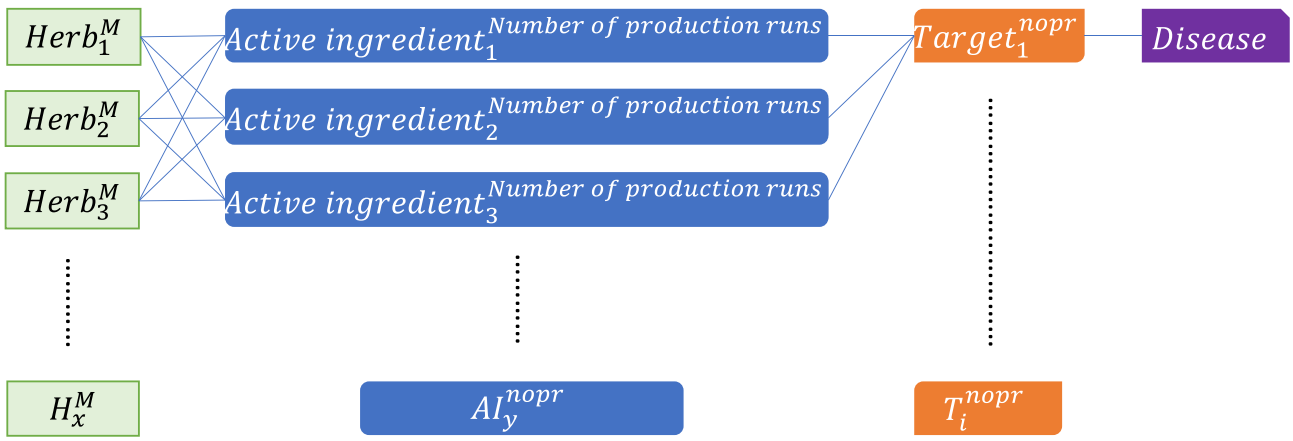

Figure 2 Schematic Network of Drug-Active Ingredient-Target-Disease.
Abbreviations: M, mass; nopr, Number of production runs.

https://doi.org/10.2147/JIR.S496124

$$Drug\ VIKOR_i^* = \left(\frac{Drug\ VIKOR_i - Drug\ VIKOR_{min}}{Drug\ VIKOR_{max} - Drug\ VIKOR_{min}}\right)$$

Intersection Target Acquisition and Final Target Scoring

Using the VENNY 2.1 tool, the intersecting targets of the three TCM formulas with the LDH targets are identified. Each target has both a disease-specific score (*LDHVIKOR*) and a drug-specific score (*DrugVIKOR*). The final target importance score (*FinalScore*) is determined by taking the weighted average of these two scores. In this study, the weights for disease and drug importance are considered equal:

$$Final\ Score_i = w_{Drug} \times Drug\ VIKOR_i^* + w_{LDH} \times LDH\ VIKOR_i$$

$$w_{Drug} = w_{LDH} = 0.5$$

Drug Scoring

Sum the *FinalScores* of the intersection targets for the three groups ($TSD \cap LDH$, $YJD \cap LDH$, $PQT \cap LDH$). The drug score ($Score_{drug}$) is the comprehensive score of the targets contained in the drug and the importance of these targets:

$$Score_{drug} = \sum_{i=1}^{\text{number of intersecting targets}} Final\ Score_i$$

Predictive Calculation of Experimental Results

The aim of this study is to evaluate whether the proposed calculation method can accurately predict the therapeutic effects of the drugs on LDH. Using the algorithm described above, the therapeutic outcomes of the intersecting targets of ($TSD \cap LDH$, $YJD \cap LDH$, $PQT \cap LDH$) are predicted. These predictions are then validated through animal experiments, which are divided into three treatment groups: TSD, YJD, and PQT (the specific dosage for each group is detailed in the animal experiment section). The steps outlined above are used to forecast the efficacy of the drugs in each experimental group, and the predictions are compared to the actual results after the experiments are completed.

GO and KEGG Enrichment Analysis of Targets

The ClusterProfiler tool was used to perform GO functional annotation and KEGG pathway enrichment analysis for the three sets of intersecting targets ($TSD \cap LDH$, $YJD \cap LDH$, $PQT \cap LDH$) independently. A significance threshold of $p < 0.05$ was applied to select relevant gene annotation categories and signaling pathways for GO functional annotation and KEGG pathway enrichment. The GO analysis was conducted across three domains: biological processes (BP), cellular components (CC), and molecular functions (MF). The top 10 results from both GO and KEGG analyses, based on enrichment significance, are presented.

Animal Experiment Validation

Experimental Animals

Twenty-five Sprague-Dawley (SD) rats, aged 6–8 weeks, were purchased from Chengdu Dashuo Laboratory Animal Co., Ltd. All animals were kept under a 12-hour light/dark cycle with controlled temperature (23 ± 1°C) and were provided with free access to food and water. The ethical approval for the animal experiments was granted under registration number SUCMDL20240304006.

Primary Experimental Materials

The Chinese medicinal herbs were obtained from the pharmacy of the Affiliated Hospital of Shaanxi University of Chinese Medicine. PQT tablets were sourced from Shaanxi Panlong Pharmaceutical Group Co., Ltd. (Shaanxi, China; specification: 0.3g×48 tablets; National Medicine Approval Number: Z61020050; product batch: 20231108). The following equipment and reagents were used: Hargreaves Infrared Plantar Test Device (Life Science, USA), Electrophoresis system (Tanon, Shanghai, China), Western blot and immunoprecipitation (IP) cell lysis buffer

(Beyotime, Shanghai, China), General protease inhibitor (Biosharp), BCA Protein Assay Kit (Beyotime, Shanghai, China), SDS-PAGE loading buffer (Biosharp), Pre-stained Protein Marker (Abclonal), PVDF membrane (Sigma-Aldrich) , Tween-20 (Servicebio), 30% Acrylamide Solution (Biosharp), HRP-conjugated Goat Anti-Mouse and Anti-Rabbit IgG (Abclonal, Affinity), GAPDH, IKK-β, and NF-κB p65 primary antibodies (Abclonal, Affinity, Proteintech), Ultra-sensitive ECL Western substrate (Zen-Bio), Molpure® RNA extraction kit (YEASEN), PrimeScript RT Reagent Kit and TB Green™ Premix Ex Taq™ II (Takara Bio Inc)., Absolute ethanol (Xilong Scientific, Sichuan), Real-time PCR and thermal cycler instruments (ThermoFisher), ELISA kits for Rat IL-1β, IL-6, IL-18, and TNF-α (Yuanju Biotechnology, Shanghai).

Establishment and Treatment of Rat LDH Model

After a 7-day acclimation period, 20 rats were randomly selected and anesthetized via intraperitoneal injection of sodium pentobarbital (50 mg/kg) and placed in a prone position. Based on a comparative study of three modeling techniques,[25] the annulus fibrosus puncture method was chosen to induce LDH in rats. The procedure involved disinfecting the rats' backs with 75% alcohol, making a longitudinal incision, and sequentially dissecting the skin, subcutaneous tissue, and lumbar fascia. After exposing the facet joints, the mammillary process was excised, and a No. 9 puncture needle was inserted at a 15° downward angle to a depth of approximately 3 mm. Upon feeling slight resistance followed by a release, 10 μL of IL-1β was injected into the disc using a microsyringe[26]. The 20 successfully modeled rats were randomly assigned to four groups: the Model group, PQT group, YJD group, and TSD group. An additional group of 5 rats, which did not undergo modeling, served as the Control group.

In this experiment, the difference in dosage was considered to lie in the concentration of the decoction rather than the volume of the liquid. Based on the literature,[27] the optimal gavage volume for rats is 10 mL/kg, and with an average rat weight of 220 g, the volume of liquid administered for gavage was fixed at 2.2 mL. The concentration of the herbal decoction was adjusted by altering the ratio of raw herbs before decoction.

The doses for the YJD and TSD groups were calculated using body surface area conversion between humans and rats[28,29]. The YJD group received 7.40 g/kg·d, and the TSD group received 3.70 g/kg·d. The required amount of raw herbs for each group was determined based on the number of animals and gavage schedule. The herbs were soaked in water for 30 minutes, then boiled for 20 minutes. After filtering, the herbs were boiled again for an additional 20 minutes. The two decoctions were combined and concentrated according to the planned gavage dosage, then refrigerated for later use. In the PQT group, the tablets were dissolved in pure water at a dose of 0.081 g/kg·d. Drug administration began 24 hours post-surgery, with the treatment groups receiving their respective drugs via gavage, while the control and model groups received the same volume of distilled water. All treatments were administered once daily for 4 weeks.

Thermal Hyperalgesia Test

Thermal hyperalgesia tests were conducted before the modeling procedure, before drug administration, and then every 7 days after the start of drug treatment for 4 weeks. Paw withdrawal latency (PWL) was measured using the Hargreaves infrared plantar stimulation device, which evaluated the thermal sensitivity of the plantar surface of the hind paw. Each animal underwent three measurements during each session, with a 5-minute interval between consecutive tests. The average of the three measurements was calculated as the thermal pain threshold. Thermal stimuli lasting 10 to 15 seconds were applied, with a 20-second limit to avoid tissue damage.[30]

H&E Staining

At the end of the drug treatment period, the rats were euthanized, and disc tissue samples were collected. The samples were placed in EDTA for decalcification, followed by embedding, sectioning, and staining with hematoxylin and eosin (H&E). After rinsing the sections with running water to remove excess stain, they were sealed and dried.

Western Blot Analysis

Rat disc tissue samples were placed into 2 mL EP tubes, with 2 grinding beads (3 mm in diameter) and RIPA lysis buffer added to each tube. The tubes were then processed using a high-speed cryogenic tissue grinder (set to −20°C) for four rounds of grinding, each lasting 60 seconds. The samples were then placed in a 4°C refrigerator for 30 minutes to allow

for lysis. Afterward, the samples were centrifuged (at 4°C, 12,000 rpm for 10 minutes), and the supernatant was collected. Protein concentrations were determined using a BCA Protein Assay Kit. The supernatant was mixed with 5× loading buffer, followed by heating at 95°C for 15 minutes to denature the proteins. The protein samples were then subjected to PAGE gel electrophoresis for separation and subsequently transferred onto a PVDF membrane. The membrane was blocked in TBST buffer containing 5% skim milk for 2 hours on a shaker at room temperature. After blocking, the membrane was washed three times with TBST, 5 minutes per wash. The membrane was then incubated overnight at 4°C with the appropriate primary antibody, diluted in blocking buffer. Following incubation, the membrane was thoroughly washed with TBST and then incubated with the secondary antibody at room temperature for 2 hours on a shaker. Protein bands were visualized using ECL chemiluminescence, and the exposed bands were captured using the Tanon Fluorescent Imaging System (version 2.0). The band intensities were analyzed using Gel-Pro Analyzer 4 software, with the results expressed as the integrated optical density (IOD) of the target proteins.

RT-PCR Experiment

Rat disc tissue samples were combined with lysis buffer in EP tubes and homogenized using a high-speed cryogenic tissue grinder. The homogenate was then transferred to an RNA adsorption column and centrifuged to collect the RNA-containing filtrate. After adding a binding buffer and mixing, the solution was transferred to a new RNA adsorption column, centrifuged again, and the filtrate was discarded. The column was washed multiple times with protein removal solution and rinse buffer, and the RNA solution was finally collected. To eliminate genomic DNA, a reaction system was prepared by mixing the Total RNA with a DNA removal reagent and incubating at 42°C for 2 minutes. A reverse transcription system was then set up to synthesize cDNA from Total RNA, which was performed in a thermal cycler. Full gene sequences were obtained from the NCBI database, and gene-specific primers were designed using Primer Premier software, synthesized by Shanghai Shenggong Biological Engineering Technology Services Co., Ltd. The PCR reaction system, along with the primers, underwent 50 cycles in a thermal cycler. The CT (Threshold cycle) values for each sample were obtained using Thermo Scientific PikoReal software, and the relative gene expression levels were calculated.

ELISA Experiment

Standard and sample wells were prepared. For each standard well, 50 μL of standard solution at varying concentrations was added. For the sample wells, 40 μL of sample dilution buffer was added, followed by 10 μL of the test sample, resulting in a 5-fold final dilution of the sample. No sample or enzyme-labeled reagent was added to the blank well, though all other steps were carried out the same. To all wells (except the blank), 100 μL of enzyme-labeled reagent was added. The plate was then sealed and incubated at 37°C for 60 minutes. A 20× concentrated washing buffer was diluted with distilled water at a 1:20 ratio. After incubation, the sealing film was carefully removed, and the liquid was discarded from the wells. Each well was washed with washing buffer, left for 30 seconds, and discarded, repeating this washing step 5 times, then blotting the plate dry. Subsequently, 50 μL of chromogenic reagent A and 50 μL of chromogenic reagent B were added to each well, mixed gently, and incubated at 37°C in the dark for 15 minutes. Afterward, 50 μL of stop solution was added to each well, stopping the reaction (the liquid color changed from blue to yellow). Finally, the absorbance at 450 nm was measured for each well using a microplate reader.

Result

Target Collection

This study included a total of 38 types of traditional Chinese medicines (with some repetitions) for drug dosage quantification. Detailed results are presented in Figure 3 and Supplementary Table 1.

After screening through the TCMSP database and additional literature sources, 732 targets were identified for TSD, 1017 targets for YJD, and 1180 targets for PQT. By integrating data from five different databases and removing duplicates, 1010 LDH-related targets were obtained, as shown in Supplementary Table 2.

Quantification of Drug Dosage				
Drug name	Accepted scientific name	Herb weight_TSD(dose)	Herb weight_YJD(dose)	Herb weight_PQT(dose)
Tao Ren	Prunus persica (L.) Batsch	4	9	\
Hong hua	Carthamus tinctorius L.	4	6	0.025
Shu Di Huang	Rehmannia glutinosa (Gaertn.) DC.	8	\	\
Bai Shao	Paeonia lactiflora Pall.	8	\	\
Dang Gui	Angelica sinensis (Oliv.) Diels	8	9	0.125
Chuan Xiong	Conioselinum anthriscoides 'Chuanxiong'	4	9	\
Sheng Di Huang	Rehmannia glutinosa (Gaertn.) DC.	\	9	\
Chuan Niu Xi	Cyathula officinalis K.C.Kuan	\	12	\
Di Long	(an annelid)-Pheretima aspergillum (E. Perrier)	\	6	\
Fu Ling	(fungus)-Wolfiporia cocos (F.A. Wolf) Ryvarden & Gilb.	\	9	\
Gan Cao	Glycyrrhiza glabra L.	\	3	\
Pan Long Qi	Bergenia scopulosa T.P.Wang	\	\	0.05
Zhuang Jin Dan	Silene tatarinowii Regel	\	\	0.01
Wu Jia Pi	Eleutherococcus nodiflorus (Dunn) S.Y.Hu	\	\	0.05
Du Zhong	Eucommia ulmoides Oliv.	\	\	0.05
Zhu Zi Shen	Panax japonicus (T.Nees) C.A.Mey.	\	\	0.005
Qing Wa Qi	Iris tectorum Maxim.	\	\	0.005
Guo Shan Long	Rhaphidophora decursiva (Roxb.) Schott	\	\	0.025
Qin Jiao	Gentiana macrophylla Pall.	\	\	0.05
Mu Xiang	Dolomiaea costus (Falc.) Kasana & A.K.Pandey	\	\	0.025
Zu Si Ma	Daphne giraldii Nitsche	\	\	0.005
Luo Shi Teng	Trachelospermum jasminoides (Lindl.) Lem.	\	\	0.025
Chuan Wu	Aconitum carmichaelii Debeaux	\	\	0.005
Bai Mao Qi	Chloranthus multistachys C.Pei	\	\	0.01
Tie Bang Chui	Aconitum pendulum N.Busch	\	\	0.005
Cao Wu	Aconitum kusnezoffii Rchb.	\	\	0.005
Lao Shu Qi	Hylomecon japonica (Thunb.) Prantl	\	\	0.01
Zhi Zhu Liao	Bistorta suffulta (Maxim.) Greene ex H.Gross	\	\	0.025
Mo Yao	Commiphora myrrha (T.Nees) Engl.	\	\	0.025
Zhu Gen Qi	Disporopsis fuscopicta Hance	\	\	0.025
Xie Cao	Valeriana officinalis L.	\	\	0.05
Shen Jin Cao	Lycopodium clavatum L.	\	\	0.01
Niu Xi	Achyranthes bidentata Blume	\	\	0.05
Dan Shen	Salvia miltiorrhiza Bunge	\	\	0.075
Yang Jiao Qi	Aconitum henryi E.Pritz. ex Diels	\	\	0.025
Ba Li Ma	Sambucus javanica Reinw. ex Blume	\	\	0.025
Chong Lou	Paris yunnanensis Franch.	\	\	0.075
Ru Xiang	Boswellia sacra Flück.	\	\	0.025

Figure 3 Quantification of Drug Dosage.

PPI Network Construction

The target sets for the three TCM formulas and LDH were imported into STRING, with the species set to "Homo sapiens" and the minimum required interaction score set to the highest confidence level (0.9). This generated PPI networks for TSD (570 nodes), YJD (811 nodes), PQT (931 nodes), and LDH (702 nodes), with the corresponding TSV files. These files were then imported into Cytoscape, where the Centiscape 2.2 plugin was used to calculate the network topology parameters: Betweenness Centrality (BC), Degree Centrality (DC), and Closeness Centrality (CC). Detailed results are presented in Supplementary Tables 3–6.

Assignment of VIKOR Values

This section selects partial data as a simple example to illustrate the detailed steps of the proposed method. Based on the calculated data in PPI Network Construction, the TSD matrix can be constructed as:

$$\boldsymbol{TSD} = \begin{bmatrix} BC & DC & CC \\ 59741.470313 & 132.000000 & 0.000729 \\ 18334.844612 & 112.000000 & 0.000669 \\ \vdots & \vdots & \vdots \\ 0.000000 & 2.000000 & 0.000250 \end{bmatrix}$$

https://doi.org/10.2147/JIR.S496124

Normalize the TSD matrix according to the normalization formula:

$$\begin{aligned} r_{11} &= v_1(c_1)/\sum_{i=1}^{570} v_i(c_1) = r_{1BC} = v_1(\mathrm{BC})/\sum_{i=1}^{570} v_i(\mathrm{BC}) \\ &= 59741.470313/(59741.470313 + 18334.844612 \cdots 0.000000) \\ &= 0.067908 \end{aligned}$$

Calculate the remaining elements of the TSD matrix, and the normalized matrix TSD_R is:

$$\boldsymbol{TSD\_R} = \begin{bmatrix} BC & DC & CC \\ 0.067908 & 0.015639 & 0.000020 \\ 0.020841 & 0.013270 & 0.000018 \\ \vdots & \vdots & \vdots \\ 0.000000 & 0.000236 & 0.000006 \end{bmatrix}$$

The weights of the network topology parameters are calculated as:

$$w_{BC} = w_{DC} = w_{CC} = 1/3$$

Determine the ideal and negative solutions according to the formula:

$$r_j^* = \{0.067908, 0.015639, 0.027601\}$$

$$r_j^- = \{0.000000, 0.000236, 0.000006\}$$

Next, calculate the utility measure and regret measure:

$$S_1 = \frac{1}{3} \times \left(\frac{0.067908 - 0.067908}{0.067908 - 0.000000}\right) + \frac{1}{3} \times \left(\frac{0.015639 - 0.015639}{0.015639 - 0.000236}\right) + \frac{1}{3} \times \left(\frac{0.027601 - 0.000020}{0.027601 - 0.000006}\right) = 0.333173$$

$$\begin{aligned} R_1 &= \max\left(\frac{1}{3} \times \left(\frac{0.067908 - 0.067908}{0.067908 - 0.000000}\right), \frac{1}{3} \times \left(\frac{0.015639 - 0.015639}{0.015639 - 0.000236}\right), \frac{1}{3} \times \left(\frac{0.027601 - 0.000020}{0.027601 - 0.000006}\right)\right) \\ &= \max(0.000000, 0.000000, 0.333173) = 0.333173 \end{aligned}$$

where:

$$S^* = min_i S_i = 0.333173$$

$$S^- = max_i S_i = 1.000000$$

$$R^* = min_i R_i = 0.333173$$

$$R^- = max_i R_i = 0.333333$$

Then, the VIKOR index is calculated as:

$$\begin{aligned} Q_1 &= \frac{v(S_1 - S^*)}{(S^- - S^*)} + \frac{(1 - v)(R_1 - R^*)}{(R^- - R^*)} \\ &= 0.5 \times \frac{0.333173 - 0.333173}{1.000000 - 0.333173} + 0.5 \times \frac{0.333173 - 0.333173}{0.333333 - 0.333173} = 0 \end{aligned}$$

Finally, transform Q:

$$Q_1^* = 1 - Q_1 = 1$$

Use the above method to calculate the TSD, YJD, PQT, and LDH matrices one by one. The specific results are shown in Supplementary Table 7.

Table 1 T_3^{nopr} Progressive Process

Herb Weight	HERB Name	Active Ingredient Name	Target Name
4	Chuanxiong	Myricanone	STAT3
4	Chuanxiong	Senkyunone	STAT3
4	Chuanxiong	Wallichilide	STAT3

Intersection Target and Weight Calculation

This section uses the data example from Assignment of VIKOR Values, selecting the well-structured data T_3^{nopr} for demonstration. The data structure is shown in Table 1.

According to the logical chain in Figure 2 and the specific values in Table 1, we have:

$$T_3^{nopr} = \sum_{x=1}^{3} AI_x^{nopr} = 12$$

After normalization:

$$w_{3,D} = \left(\frac{T_3^{nopr} - T_{min}^{nopr}}{T_{max}^{nopr} - T_{min}^{nopr}}\right) = \left(\frac{12 - 0.005}{558 - 0.005}\right) = 0.021496$$

After intersecting the TSD, YJD, and PQT target sets with the LDH target set, we obtain 167 $TSD \cap LDH$ targets, 210 $YJD \cap LDH$ targets, and 220$PQT \cap LDH$ targets. The intersection targets have both *LDHVIKOR* and *DrugVIKOR*,

$$Drug\ VIKOR_3 = w_{3,D} \times Q_{3,D}^{*} = 0.021496 \times 0.694710 = 0.014933$$

$$LDH\ VIKOR_3 = w_{3,L} \times Q_{3,L}^{*} = 1 \times 0.761259 = 0.761259$$

Thus:

$$Drug\ VIKOR_3^{*} = \left(\frac{Drug\ VIKOR_3 - Drug\ VIKOR_{min}}{Drug\ VIKOR_{max} - Drug\ VIKOR_{min}}\right) = \left(\frac{0.014933 - 0}{0.140431 - 0}\right) = 0.106343$$

$$\begin{aligned} Final\ Score_3 &= w_{Drug} \times Drug\ VIKOR_3^{*} + w_{LDH} \times LDH\ VIKOR_3 \\ &= 0.5 \times 0.106343 + 0.5 \times 0.761259 = 0.433801 \end{aligned}$$

Using the above method, calculate the *FinalScores* for the three groups of intersection targets ($TSD \cap LDH$, $YJD \cap LDH$, $PQT \cap LDH$). The specific results are shown in Supplementary Table 8.

Summing the target scores for each group, the predicted experimental results are as follows:

$$Score_{TSD} = \sum_{i=1}^{167} Final\ Score_i = 32.459158$$

$$Score_{YJD} = \sum_{i=1}^{210} Final\ Score_i = 39.968154$$

$$Score_{PQT} = \sum_{i=1}^{220} Final\ Score_i = 39.916694$$

Based on these results, the predicted treatment efficacy ranks as YJD > PQT > TSD, with YJD and PQT showing highly similar effectiveness.

https://doi.org/10.2147/JIR.S496124

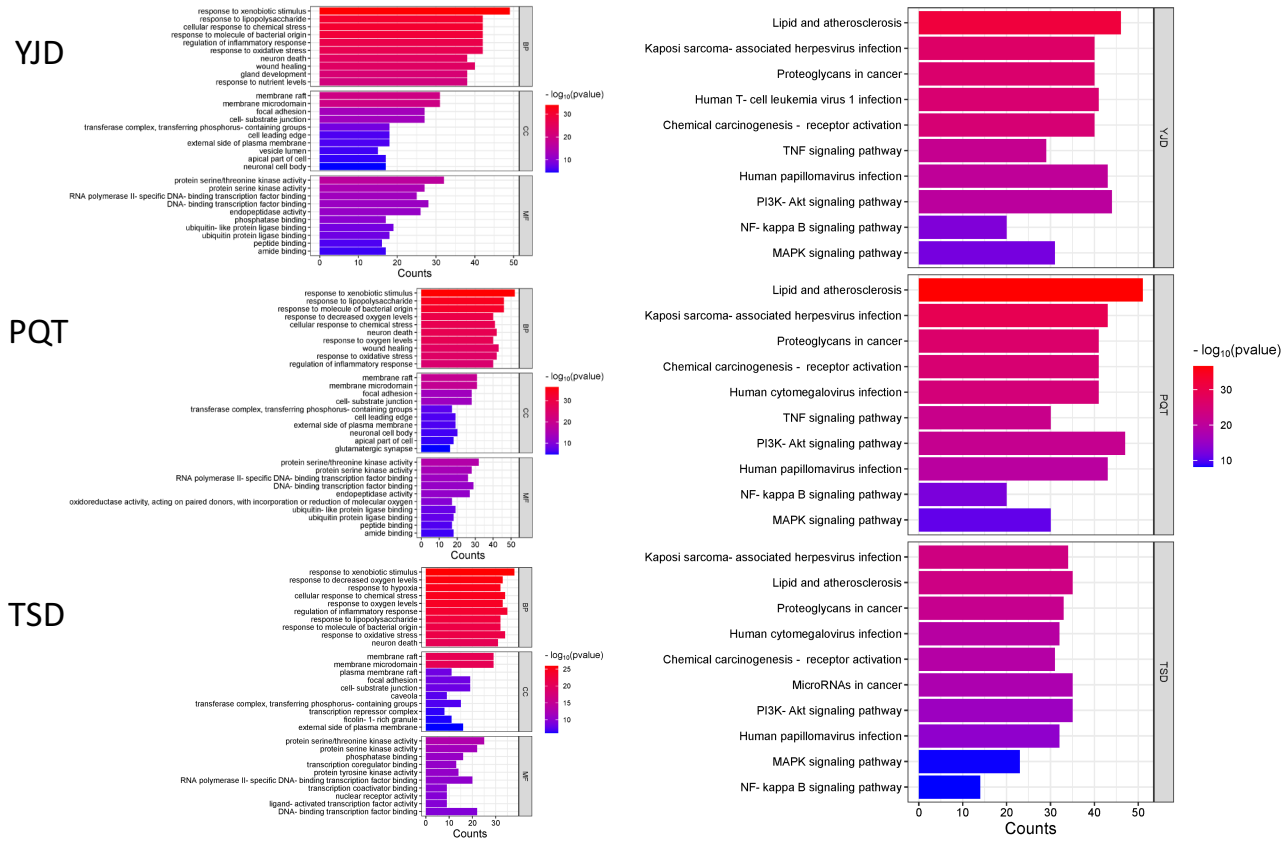

Figure 4 Comparative GO and KEGG Enrichment Analysis of the Three Intersecting Target Sets.
Abbreviations: YJD, Yaotong Jizheng Decoction; PQT, Panlong Qi Tablet; TSD, Taogong Siwu Decoction.

GO and KEGG Enrichment Analysis

The intersecting target sets ($TSD \cap LDH$, $YJD \cap LDH$, $PQT \cap LDH$) were individually analyzed using ClusterProfiler for GO enrichment across biological process (BP), cellular component (CC), and molecular function (MF). The comparative results are displayed in Figure 4.

GO and KEGG analyses indicated a significant overlap in biological processes and signaling pathways among the three groups of intersecting targets, with many terms related to oxidative stress, inflammatory responses, and their associated pathways. All three groups were notably involved in the PI3K-Akt, MAPK, and NF-kappa B signaling pathways, which play key roles in inflammation and cellular stress responses.

Thermal Hyperalgesia Test and H&E Staining

As shown in Figure 5A, no significant differences were observed between the model group and the treatment groups before the 7th day of drug intervention ($P > 0.05$). From the 7th day onwards, the YJD group demonstrated a statistically significant difference compared to the model group ($P < 0.05$). By the 14th day, both the YJD and PQT groups exhibited significant differences compared to the model and TSD groups ($P < 0.05$), while the TSD group remained statistically similar to the model group. After 28 days of treatment, all treatment groups showed significant differences compared to the model group ($P < 0.05$), and the difference between the YJD group and the control group disappeared ($P > 0.05$). Detailed results are provided in Supplementary Table 9.

In the H&E staining analysis (Figure 5B), the model group showed lower cell density and more pronounced degeneration compared to the control group. Among the treatment groups, YJD and PQT exhibited tissue morphology more similar to the control group, while TSD showed characteristics closer to the model group. Taken together, the

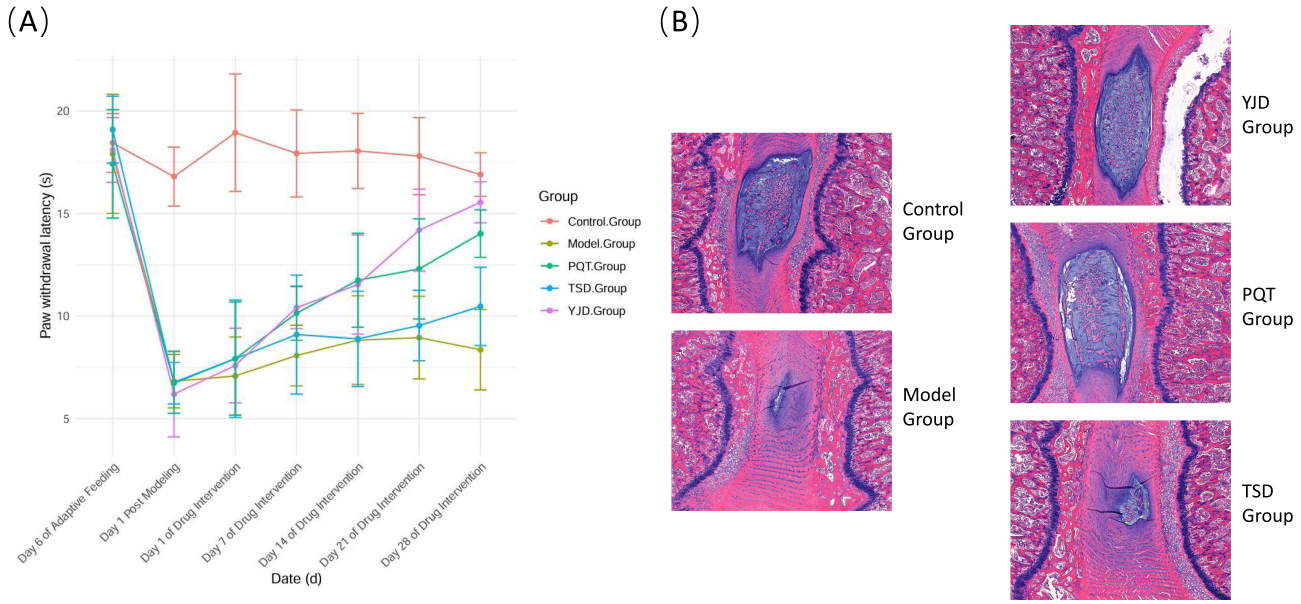

Figure 5 Comparative Analysis of Thermal Pain Threshold (**A**) and H&E Staining Results (**B**).
Abbreviations: YJD, Yaotong Jizheng Decoction; PQT, Panlong Qi Tablet; TSD, Taogong Siwu Decoction.

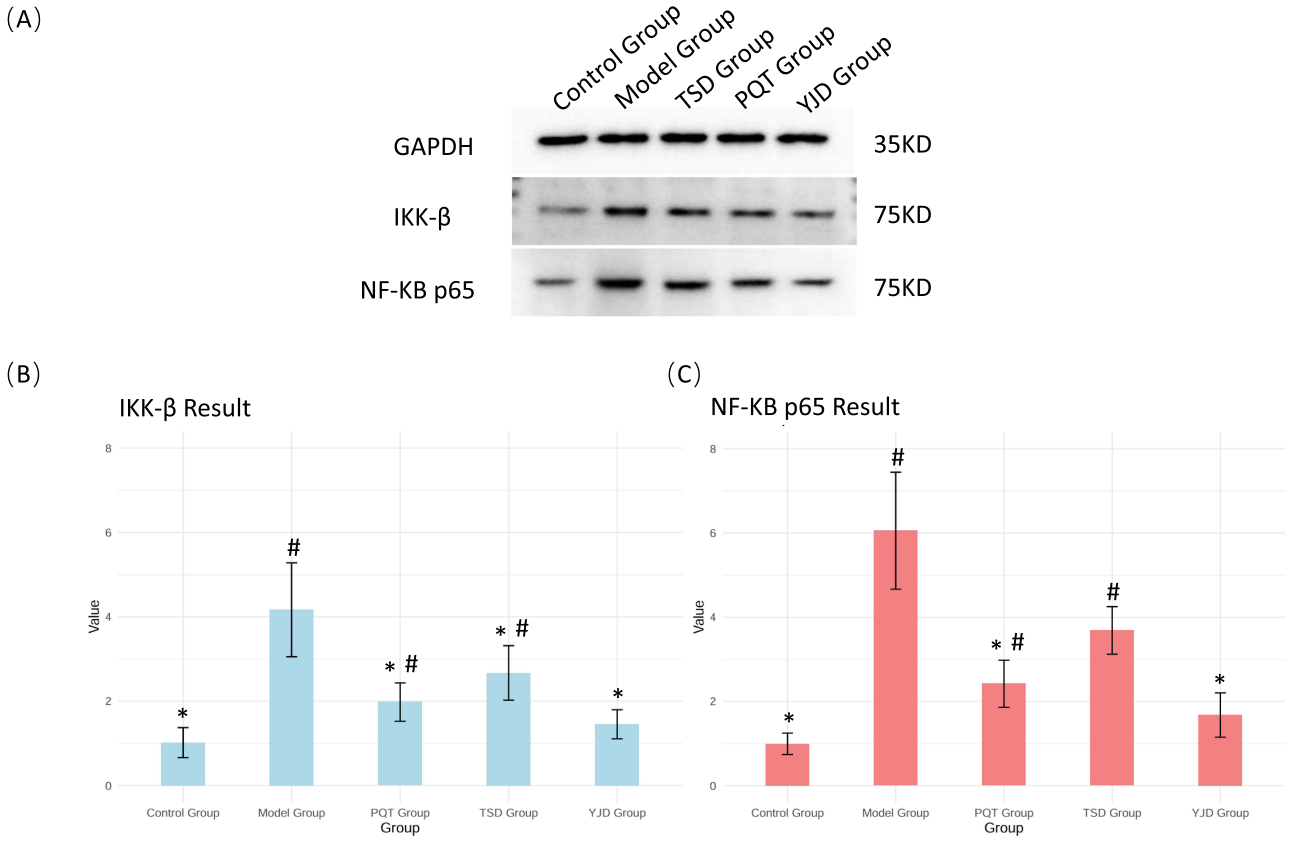

Figure 6 Protein Expression in Rat Tissues. (**A**) Western blot analysis of relevant proteins (IKK-β and NF-κB p65) in rat tissues. (**B**) Expression levels of IKK-β across groups. (**C**) Expression levels of NF-κB p65 across groups. "#" indicates a statistically significant difference compared to the control group ($P < 0.05$); "*" indicates a statistically significant difference compared to the model group ($P < 0.05$).

https://doi.org/10.2147/JIR.S496124

thermal hyperalgesia test and H&E staining results confirm successful modeling and suggest a preliminary gradient of treatment efficacy among the groups.

Western Blot Analysis

The expression of IKK-β and NF-κB p65 proteins in rat tissues across different groups is shown in Figure 6A and B.

Compared to the control group, the model group exhibited significantly increased levels of both IKK-β and NF-κB p65 ($P < 0.05$). Among the treatment groups, only the TSD group showed no significant difference in NF-κB p65 expression compared to the model group ($P > 0.05$). Notably, the YJD group showed significant differences in the expression of both proteins compared to the TSD group and displayed no statistical difference from the healthy control group ($P > 0.05$).

RT-PCR Analysis

The primers and nucleotide sequences used in this experiment are listed in Table 2.

The mRNA expression levels in rat tissues for each group are displayed in Figure 7.

Compared to the control group, the model group exhibited significant differences in mRNA expression for IKK, IKB, NLRP3, and caspase-1. In the YJD group, significant differences were observed in IKK, NLRP3, and caspase-1 expression compared to the model group, except for IKB ($P < 0.05$). The PQT and TSD groups did not show significant differences in any of the four markers compared to the model group. Among the treatment groups, a significant difference in caspase-1 expression was observed between the YJD and TSD groups.

ELISA Analysis

The ELISA detection results for IL-1β, IL-6, IL-18, and TNF-α are presented in Figure 8.

Compared to the control group, the model group showed significant increases in IL-1β, IL-6, IL-18, and TNF-α levels. In the TSD group, significant differences were observed in IL-1β, IL-18, and TNF-α, while the PQT group showed a significant difference only in TNF-α. However, compared to the model group, the TSD group did not exhibit significant differences in IL-1β, IL-18, or TNF-α levels. Among the treatment groups, a significant difference in IL-18 levels was found between the YJD and TSD groups.

Discussion

Previous studies indicate that LDH typically begins at an average age of 40 to 45 years[31–33] According to the TCM classic "Shanggu Tianzhen Lun", it is stated, "At six sevens (age 42), the three Yang meridians decline in women, the face becomes haggard, and hair begins to turn white", and "At five eights (age 40), the kidney Qi declines in men, causing hair loss and teeth to wither". This indicates that the age range of 40–45 already shows a gradual weakening of physical functions, especially in women. This was strongly supported by the fact that in the study of 353 patients in 2020[34] and 149 patients in 2023,[35] over 55% of the female patients were in this age range. Combining these points from a TCM perspective, most LDH patients face not only pain caused by Qi and blood stasis but also physical depletion. Therefore, Dr. Yang Lixue, a renowned TCM doctor in Shaanxi Province, has, through many years of clinical practice,

Table 2 Primers and Nucleotide Sequences

Primer Name	Forward Sequence	Reverse Sequence
β-actin	gggaaatcgtgcgtgacatt	gcggcagtggccatctc
caspase-1	aaacacccactcgtacacgtcttg	aggtcaacatcagctccgactctc
IKB	ttggtgactttgggtgctgatg	cacacttcaacaggagcgagac
IKK	gacctagaggaacaagcaagagaac	agcagcagccgtaccatatcc
NLRP3	agacctccaagaccacgactg	ttccatccgcagccaatgaac

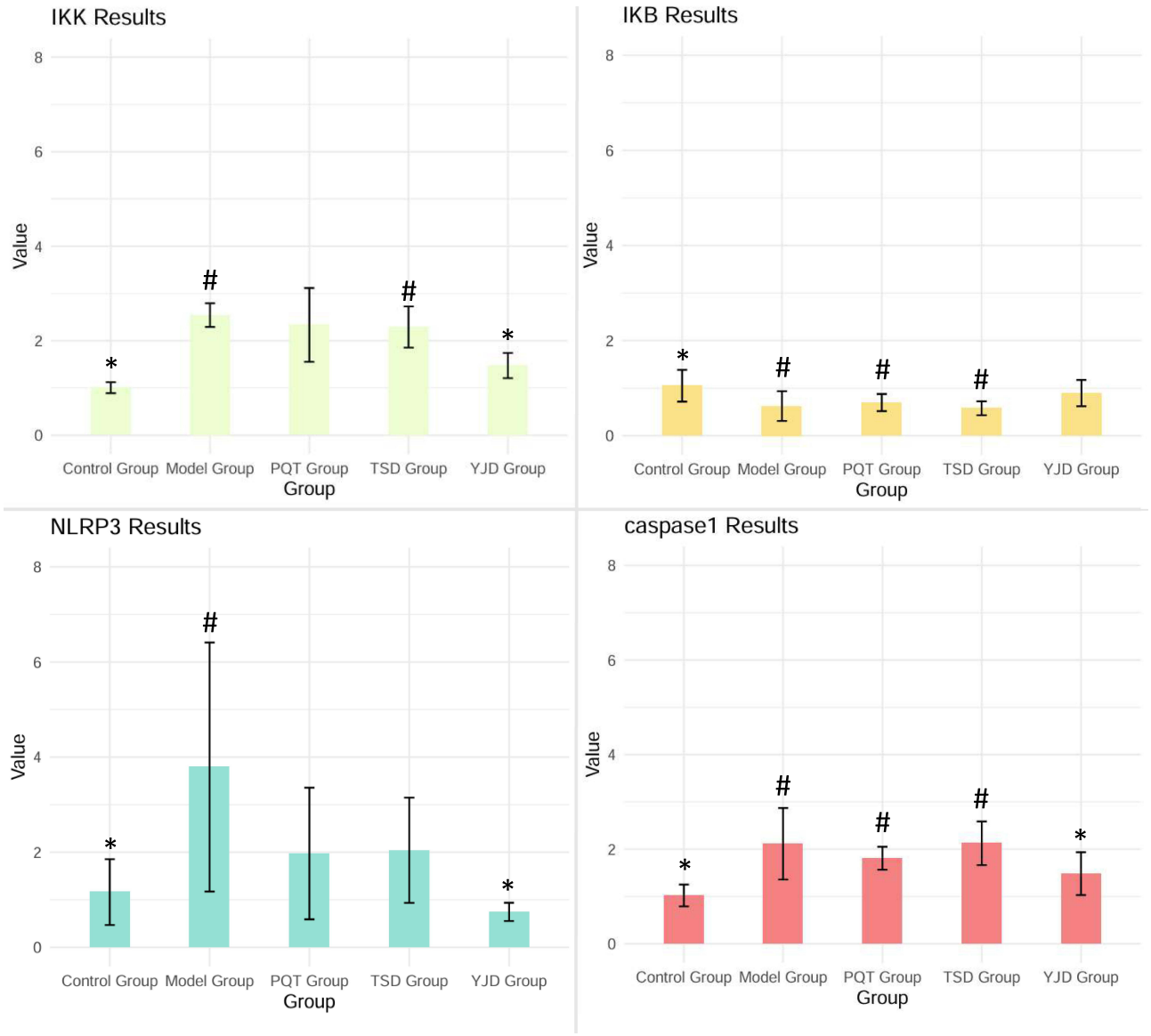

Figure 7 mRNA Expression in Rat Tissues. "#" indicates a statistically significant difference compared to the control group ($P < 0.05$); "*" indicates a statistically significant difference compared to the model group ($P < 0.05$).

used TSD as a base formula to promote blood circulation. He modified the formula by adding herbs that nourish Yin and replenish blood according to the characteristics of the patient group, resulting in a new formulation, YJD, which is more suitable for the LDH population and specifically targets LDH symptoms. The positive control drug selected in this study, PQT, is an anti-inflammatory and analgesic drug that has been extensively studied[36,37] and has long been used in clinical practice.

The experimental results indicate that the formulas YJD, PQT, and TSD show significant similarity in GO and KEGG pathway analyses, with all three formulas modulating LDH through mechanisms related to oxidative stress and inflammation. Oxidative stress arises from excessive production of reactive oxygen species (ROS) or an insufficient antioxidant defense. Excessive ROS activates the NF-κB and MAPK signaling pathways, disrupting the balance between degradation and synthesis of the extracellular matrix in intervertebral disc cells, while also promoting the secretion of pro-inflammatory factors. These alterations lead to the loss of intervertebral disc cells and establish a persistent inflammatory microenvironment, further degrading disc tissue[38]. In addition, the expression of inflammatory mediators such as IL-1β and TNF-α is strongly associated with disc degeneration and herniation.[2,39] According to the GO and

https://doi.org/10.2147/JIR.S496124

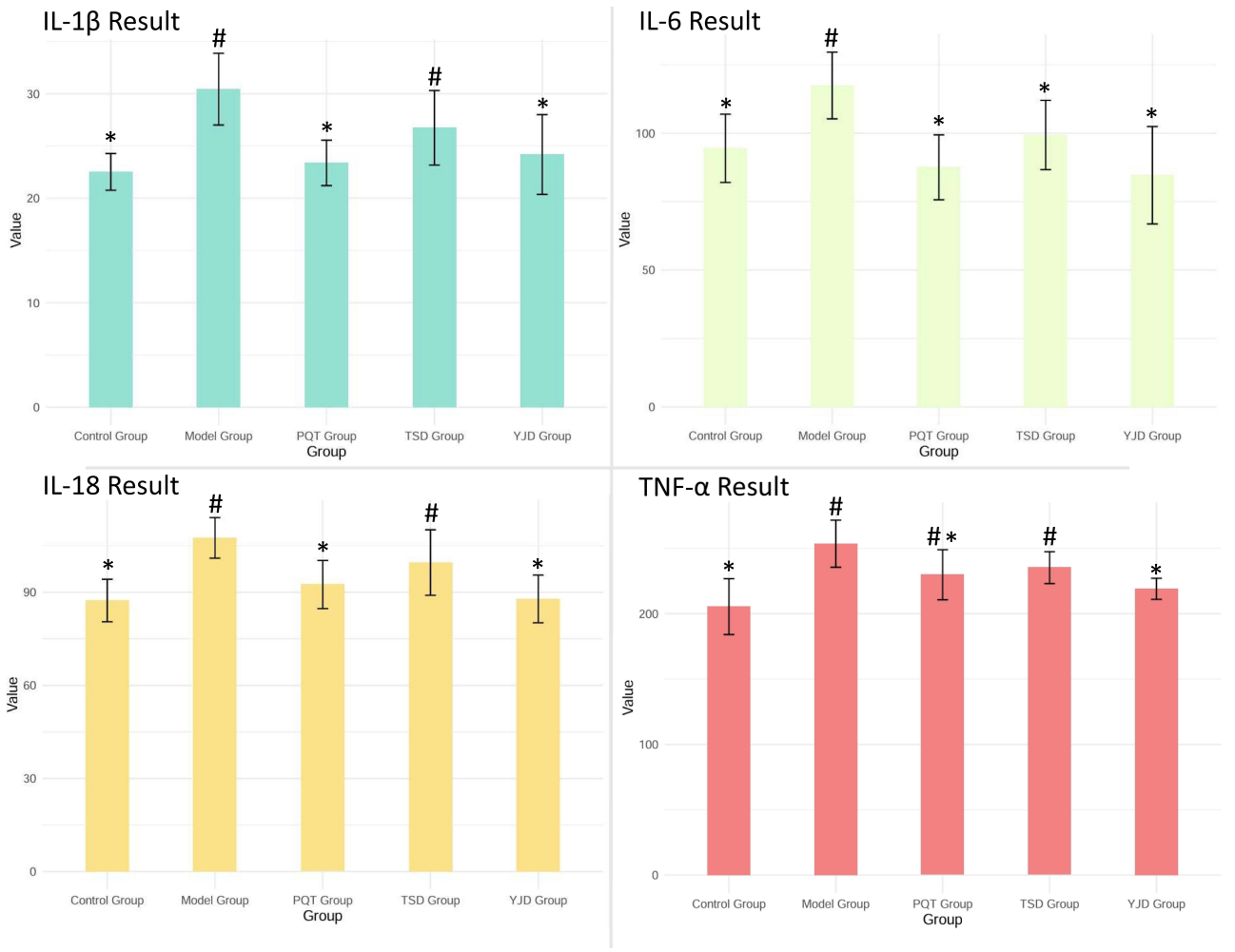

Figure 8 ELISA Results. "#" indicates a statistically significant difference compared to the control group (P < 0.05); "*" indicates a statistically significant difference compared to the model group (P < 0.05).

KEGG enrichment analyses, several pathways were highly enriched, including the PI3K-Akt signaling pathway, MAPK signaling pathway, and NF-κB signaling pathway. These pathways are considered key areas for further investigation due to their relevance to LDH pathology.

The results from the three assays show that after activation, IKK-β (as detected by Western Blot, WB) becomes phosphorylated and degrades IKB (RT-PCR), allowing NF-κB p65 (WB) to be released and translocated into the nucleus, where it activates the expression of downstream inflammatory genes, including IL-1β (ELISA), IL-6 (ELISA), and TNF-α (ELISA)[40]. NF-κB p65 also promotes the expression of the NLRP3 gene (RT-PCR), which increases its assembly into inflammasomes and activates caspase-1, leading to the maturation and release of pro-inflammatory cytokines IL-1β (ELISA) and IL-18 (ELISA) into the extracellular space[41,42]. Additionally, TNF-α and IL-6 can feedback to further activate NF-κB p65, forming a continuous positive feedback loop.[40] At the upstream level of this signaling cascade, the detection of IKK and IKK-β revealed that YJD showed results comparable to the control group. In the IKK-β assay, YJD showed statistically significant differences from TSD while being on par with PQT. IKB degradation was minimal in the YJD group, closely resembling the control group. Similarly, the NF-κB p65 results paralleled those of IKK-β, with YJD showing the best performance among the three groups: YJD > TSD and YJD ≈ PQT. In subsequent experiments involving NLRP3, caspase-1, inflammatory factors, and H&E staining, YJD continued to show results similar to the control group and comparable to PQT, with a significant advantage over TSD. Furthermore, the results from thermal

hyperalgesia experiments showed that YJD was closest to the control group among the three treatment groups. These findings align with the initial computational predictions, confirming the algorithm's validity in animal experiments.

The algorithm proposed in this study is based on a PPI network, which is composed of the interactions between proteins. These interactions play critical roles in various biological processes and are fundamental for understanding disease mechanisms and developing new therapies.[43,44] Previous research in network pharmacology often relies on PPI networks to model drug-disease interactions,[45] using network topology parameters to assess the importance of each node. Building upon these prior studies, our research integrates multiple network topology parameters to create a comprehensive scoring system. In this system, the dosage of each drug is progressively passed to the target proteins, allowing for an importance-weighted score. Despite these advancements, this study still faces limitations, particularly in the idealization of the model, as constructing a precise database of drug active ingredient output is a substantial challenge. To address this, we revised our approach by independently decomposing the weights and converting them into frequencies, which allowed us to create a more refined model. Moreover, we externalized all the weights in the algorithm, enabling researchers to adjust the importance of specific parameters or components based on their quantitative results and understanding. This flexibility helps achieve predictions that better align with clinical realities. Rather than introducing a completely new evaluation system, this study functions as a numerical aggregation of multiple dimensions. The core evaluation framework remains based on the traditional, well-established system, with the innovation being the expanded data range. By distinguishing between two key aspects—identifying which targets are most critical for treating LDH and determining which drug formulas can best address those targets—we were able to aggregate these insights into a more comprehensive predictive model.

When all drug dosages are set at standard clinical levels, YJD and PQT demonstrated a clear advantage over TSD in the calculations. However, the variation in the number of compounds remains an important confounding factor. While YJD and TSD have a similar number of ingredients, YJD's total dosage is nearly twice that of TSD. In contrast, PQT dosages only about one-fortieth of TSD, yet contains five times as many different compounds. In traditional network pharmacology, an increase in the number of compounds generally expands the range of potential therapeutic targets, leading to greater overlap with disease-related targets. Although impractical in real-world applications, from a purely theoretical network pharmacology standpoint, taking all herbal medicines at once could potentially activate numerous unnecessary targets, but it would bring the treatment closer to activating all the targets associated with the disease. However, activating targets related to conditions such as cancer while treating LDH could have catastrophic consequences in clinical practice. For this reason, the number of compounds in a treatment should be carefully limited to activate only the most critical targets while minimizing unnecessary ones. In this study, YJD targeted significantly more LDH-related sites than TSD, approaching the efficiency of PQT. However, the difference in the number of ingredients between PQT and YJD—29 compared to 9—suggests that YJD may be near the optimal efficiency point for treating LDH with TCM. This principle, known in TCM as "fewer medicines, stronger effects", refers to achieving maximum therapeutic results with the minimum number of ingredients.

Combining the results of animal experiments with our group's previous research, it is suggested that while TSD theoretically has some therapeutic potential for treating LDH,[46] its actual effectiveness is quite limited[47]. Long-term clinical observations also indicate that patients tend to show a stronger preference and greater willingness to cooperate with YJD and PQT treatments, rather than with TSD. Given these observations, we have reason to believe that, despite the inherent challenges of network pharmacology—such as issues with data updates and synergistic effects—placing it at some distance from direct clinical application, the computational results offer valuable insights as an initial screening strategy. These results help clarify certain aspects of clinical efficacy, allowing for theoretical simulations to compare the potential effects of different treatment formulas.

Conclusion

This study introduced dosage as a new factor into network pharmacology research, and the results preliminarily demonstrated the potential of using a comprehensive scoring algorithm to compare different formulas at standard clinical doses. This approach offers valuable insights for the future design and evaluation of treatment formulas. However, due to the inherent limitations of network pharmacology and current detection technologies, dosage control in clinical practice still requires significant reliance on

physicians' expertise and extensive data. In the future, the development of a specialized database could further enhance our algorithm, enabling the expansion of computer-aided drug design (CADD) in the field of targeted treatment.

Abbreviations

BC, Betweenness Centrality; BCA, Bicinchoninic Acid; BP, Biological Process; CADD, Computer-Aided Drug Design; CC, Closeness Centrality/Cellular Component; CTD, Comparative Toxicogenomics Database; DC, Degree Centrality; DL, Drug-Likeness; DRG, Dorsal Root Ganglion; ECL, Enhanced Chemiluminescence; GO, Gene Ontology; HRP, Horseradish Peroxidase; KEGG, Kyoto Encyclopedia of Genes and Genomes; LDH, Lumbar Disc Herniation; MAPK, Mitogen-Activated Protein Kinase; MCDM, Multi-Criteria Decision Making; NCBI, National Center for Biotechnology Information; OB, Oral Bioavailability; PAGE, Polyacrylamide Gel Electrophoresis; PPI, Protein-Protein Interaction; PQT, Panlong Qi Tablet.

PMSF, Phenylmethylsulfonyl Fluoride; PWL, Paw Withdrawal Latency; ROS, Reactive Oxygen Species; SD, Sprague-Dawley (a breed of rats); STRING, Search Tool for the Retrieval of Interacting Genes/Proteins; TSD, Taohong Siwu Decoction; TBST, Tris-Buffered Saline with Tween 20; TCM, Traditional Chinese Medicine; TCMSP, Traditional Chinese Medicine Systems Pharmacology; VIKOR, Vlsekriterijumska Optimizacija I Kompromisno Resenje (Multicriteria Optimization and Compromise Solution); WB, Western Blot; YJD, Yaotong Jizheng Decoction; H&E, Hematoxylin and Eosin staining; ELISA, Enzyme-Linked Immunosorbent Assay; RT-PCR, Reverse Transcription Polymerase Chain Reaction; Tec, target evaluation criteria.

Ethics Statement

This study was conducted in accordance with the ethical standards of the Institutional Ethics Committee. The animal experimentation protocol was reviewed and approved by the Institutional Animal Ethics Committee of Shaanxi University of Chinese Medicine (Approval No. SUCMDL20240304006), in accordance with the national standard GB/T 35892-2018: Laboratory Animal Welfare and Ethical Review Guidelines.

Acknowledgments

We extend our sincere appreciation to the database administrators for their essential maintenance and support, which have been critical to the success of this research. We are particularly grateful to Scholar Yuanzhi Yang for providing essential algorithmic references that substantially enhanced our study.

Author Contributions

All authors made a significant contribution to the work reported, whether that is in the conception, study design, execution, acquisition of data, analysis, and interpretation, or in all these areas; took part in drafting, revising, or critically reviewing the article; gave final approval of the version to be published; have agreed on the journal to which the article has been submitted; and agree to be accountable for all aspects of the work.

Funding

This work was supported by the National Natural Science Foundation project (No. 81973889).

Disclosure

The authors declare that they have no competing interests in this work.

References

1. Albeck MJ. A critical assessment of clinical diagnosis of disc herniation in patients with monoradicular sciatica. *Acta neurochirurgica*. 1996;138:40–44. doi:10.1007/BF01411722
2. Cunha C, Silva AJ, Pereira P, Vaz R, Gonçalves RM, Barbosa MA. The inflammatory response in the regression of lumbar disc herniation. *Arthritis Res Therapy*. 2018;20(1):251. doi:10.1186/s13075-018-1743-4
3. Gadjradj PS, Smeele NVR, de Jong M, et al. Patient preferences for treatment of lumbar disc herniation: a discrete choice experiment. *J Neurosurg Spine*. 2022;36(5):704–712. doi:10.3171/2021.8.SPINE21995

4. Sillevis R, Cuenca-Zaldívar JN, Fernández-Carnero S, García-Haba B, Sánchez Romero EA, Selva-Sarzo F. Neuromodulation of the autonomic nervous system in chronic low back pain: a randomized, controlled, crossover clinical trial. *Biomedicines*. 2023;11(6):1551. doi:10.3390/biomedicines11061551
5. Qin X, Sun K, Xu W, et al. An evidence-based guideline on treating lumbar disc herniation with traditional Chinese medicine. *J Evid Based Med*. 2024;17(1):187–206. doi:10.1111/jebm.12598
6. Wang M, Yin F, Kong L, et al. Chinmedomics: a potent tool for the evaluation of traditional Chinese medicine efficacy and identification of its active components. *ChinMed*. 2024;19(1):47. doi:10.1186/s13020-024-00917-x
7. Marshall AC. *Traditional Chinese Medicine and Clinical Pharmacology*. Springer; 2020.
8. Han Q, Li Z, Fu Y, et al. Analyzing the research landscape: mapping frontiers and hot spots in anti-cancer research using bibliometric analysis and research network pharmacology. *Front Pharmacol*. 2023;14:1256188. doi:10.3389/fphar.2023.1256188
9. Yang Y, Yu L, Wang X, et al. A novel method to evaluate node importance in complex networks. *Phys A*. 2019;526:121118. doi:10.1016/j.physa.2019.121118
10. Ru J, Li P, Wang J, et al. TCMSP: a database of systems pharmacology for drug discovery from herbal medicines. *J Cheminf*. 2014;6:13. doi:10.1186/1758-2946-6-13
11. Liang X, Li Y, Fan H, et al. Chemical constituents from the roots and rhizomes of Silene tatarinowii Regel. *Biochem Syst Ecol*. 2019;86:103932. doi:10.1016/j.bse.2019.103932
12. Xiangyu C, Jinghan Z, Jiahao L, Wenli Z, Zhigang M, Huifang N. Study on the medication pattern and its mechanism of action of Yiqi and blood-activating prescriptions against cerebral ischemia/reperfusion injury based on data mining. *Chin Herb Med*. 2023;54(10):3221–3236.
13. Xin L, Minggu S, Xiaoliang Z, Jia L. Exploring the medication pattern and mechanism of action of Yin-deficient immune thrombocytopenia based on literature mining and network pharmacology. *J Liaoning Univ Traditional Chin Med*. 2024;26(02):19–25.
14. Kim S, Thiessen PA, Bolton EE, et al. PubChem Substance and Compound databases. *Nucleic Acids Res*. 2016;44(D1):D1202–1213. doi:10.1093/nar/gkv951
15. Daina A, Michielin O, Zoete VJ. SwissTargetPrediction: updated data and new features for efficient prediction of protein targets of small molecules. *Nucleic Acids Res*. 2019;47(W1):W357–W364. doi:10.1093/nar/gkz382
16. Stelzer G, Rosen N, Plaschkes I, et al. The GeneCards Suite: from gene data mining to disease genome sequence analyses. *Curr protoc bioinf*. 2016;54:1.30.31–31.30.33. doi:10.1002/cpbi.5
17. Piñero J, Ramírez-Anguita JM, Saüch-Pitarch J, et al. The DisGeNET knowledge platform for disease genomics: 2019 update. *Nucleic Acids Res*. 2020;48(D1):D845–D855. doi:10.1093/nar/gkz1021
18. Amberger JS, Bocchini CA, Schiettecatte F, Scott AF, Hamosh AJ. OMIM. org: Online Mendelian Inheritance in Man (OMIM®), an online catalog of human genes and genetic disorders. *Nucleic Acids Res*. 2015;43(D1):D789–D798. doi:10.1093/nar/gku1205
19. Brown GR, Hem V, Katz KS, et al. Gene: a gene-centered information resource at NCBI. *Nucleic Acids Res*. 2015;43(D1):D36–D42. doi:10.1093/nar/gku1055
20. Davis AP, Wiegers TC, Johnson RJ, Sciaky D, Wiegers J, Mattingly CJJ. Comparative toxicogenomics database (CTD): update 2023. *Nucleic Acids Res*. 2023;51(D1):D1257–D1262. doi:10.1093/nar/gkac833
21. Shao L, Zhang BJC. Traditional Chinese medicine network pharmacology: theory, methodology and application. *Chin J Nat Med*. 2013;11(2):110–120. doi:10.1016/S1875-5364(13)60037-0
22. Brambila B, Martelli ACFS, Barcelos MP, Antão SC, da Silva CHTP, Novo-Mansur MTM. Protein–protein interaction for drug discovery. In: Taft CA, de Almeida PF, editors. *Trends and Innovations in Energetic Sources, Functional Compounds and Biotechnology: Science, Simulation, Experiments*. Cham: Springer Nature Switzerland; 2024:255–269.
23. Szklarczyk D, Kirsch R, Koutrouli M, et al. The STRING database in 2023: protein-protein association networks and functional enrichment analyses for any sequenced genome of interest. *Nucleic Acids Res*. 2023;51(D1):D638–D646. doi:10.1093/nar/gkac1000
24. Fan W, He Y, Han X, Feng YJ. A new model to identify node importance in complex networks based on DEMATEL method. *Sci Rep*. 2021;11(1):22829. doi:10.1038/s41598-021-02306-y
25. Yin H, Ji M, Hu Z, et al. Comparison and evaluation of three lumbar intervertebral disc herniation rat model preparation methods. *Chin J Tissue Eng Res*. 2025; 29(14):2930–2936.
26. Kim H, Hong JY, Lee J, Jeon WJ, Ha IH. IL-1β promotes disc degeneration and inflammation through direct injection of intervertebral disc in a rat lumbar disc herniation model. *Spine J*. 2021;21(6):1031–1041. doi:10.1016/j.spinee.2021.01.014
27. Gad SC, Spainhour CB, Shoemake C, et al. Tolerable levels of nonclinical vehicles and formulations used in studies by multiple routes in multiple species with notes on methods to improve utility. *Int J Toxicol*. 2016;35(2):95–178. doi:10.1177/1091581815622442
28. Wang ZY, Li MZ, Li WJ, Ouyang JF, Gou XJ, Huang Y. Mechanism of action of Daqinjiao decoction in treating cerebral small vessel disease explored using network pharmacology and molecular docking technology. *Phytomedicine*. 2023;108:154538. doi:10.1016/j.phymed.2022.154538
29. Wojcikowski K, Gobe G. Animal studies on medicinal herbs: predictability, dose conversion and potential value. *Phytother Res*. 2014;28(1):22–27. doi:10.1002/ptr.4966
30. Xu W, Ding W, Sheng H, Lu D, Xu X, Xu B. Dexamethasone suppresses radicular pain through targeting the L-PGDS/PI3K/Akt pathway in rats with lumbar disc herniation. *Pain Pract*. 2021;21(1):64–74. doi:10.1111/papr.12934
31. Fidan F, Balaban M, Hatipoğlu ŞC, Veizi E. Is lumbosacral transitional vertebra associated with lumbar disc herniation in patients with low back pain? *Eur Spine J*. 2022;31(11):2907–2912. doi:10.1007/s00586-022-07372-y
32. Tian G, Wang Y, Xia J, et al. Correlation of multifidus degeneration with sex, age and side of herniation in patients with lumbar disc herniation. *BMC Musculoskelet Disord*. 2023;24(1):652. doi:10.1186/s12891-023-06783-2
33. Geng J, Wang L, Li Q, et al. The Association of Lumbar Disc herniation with lumbar volumetric bone mineral density in a cross-sectional Chinese Study. *Diagnostics*. 2021;11(6):938. doi:10.3390/diagnostics11060938
34. Yao M, Xu BP, Li ZJ, et al. A comparison between the low back pain scales for patients with lumbar disc herniation: validity, reliability, and responsiveness. *Health Qual Life Outcomes*. 2020;18(1):175. doi:10.1186/s12955-020-01403-2
35. Cuenca-Zaldívar JN, Fernández-Carnero J, Sánchez-Romero EA, et al. Effects of a therapeutic exercise protocol for patients with chronic non-specific back pain in Primary Health Care: a Single-Group Retrospective Cohort Study. *J Clin Med*. 2023;12(20):6478. doi:10.3390/jcm12206478

36. Niu X, Yang Y, Yu J, et al. Panlongqi tablet suppresses adjuvant-induced rheumatoid arthritis by inhibiting the inflammatory reponse in vivo and in vitro. *J Ethnopharmacol*. 2023;308:116250. doi:10.1016/j.jep.2023.116250
37. Wang L, Xu P, Xu Y, et al. A discovery of clinically approved Panlongqi Tablet for repositioning to treat osteoarthritis by inhibiting PI3K/AKT activation. *Phytomedicine*. 2022;105:154360. doi:10.1016/j.phymed.2022.154360
38. Kang L, Zhang H, Jia C, Zhang R, Shen C. Targeting oxidative stress and inflammation in intervertebral disc degeneration: therapeutic perspectives of phytochemicals. *Front Pharmacol*. 2022;13:956355. doi:10.3389/fphar.2022.956355
39. Chen X, Wang Z, Deng R, Yan H, Liu X, Kang R. Intervertebral disc degeneration and inflammatory microenvironment: expression, pathology, and therapeutic strategies. *Inflammation Res*. 2023;72(9):1811–1828. doi:10.1007/s00011-023-01784-2
40. Karin M. How NF-κB is activated: the role of the IκB kinase (IKK) complex. *Oncogene*. 1999;18(49):6867–6874. doi:10.1038/sj.onc.1203219
41. Gan J, Guo L, Zhang X, et al. Anti-inflammatory therapy of atherosclerosis: focusing on IKKβ. *J Inflam*. 2023;20(1):8. doi:10.1186/s12950-023-00330-5
42. Solt LA, May MJ. The IκB kinase complex: master regulator of NF-κB signaling. *Immunol Res*. 2008;42(1):3–18. doi:10.1007/s12026-008-8025-1
43. Gustafsson M, Nestor CE, Zhang H, et al. Modules, networks and systems medicine for understanding disease and aiding diagnosis. *Genome Med*. 2014;6(10):82. doi:10.1186/s13073-014-0082-6
44. Rout T, Mohapatra A, Kar M. A systematic review of graph-based explorations of PPI networks: methods, resources, and best practices. *Network Model Anal Health Inf Bioinf*. 2024;13(1):29. doi:10.1007/s13721-024-00467-0
45. Noor F, Tahir Ul Qamar M, Ashfaq UA, Albutti A, Alwashmi ASS, Aljasir MA. Network pharmacology approach for medicinal plants: review and assessment. *Pharmaceuticals*. 2022;15(5):572. doi:10.3390/ph15050572
46. Luchun X, Jianjun W, Huainan L. Network pharmacological mechanism of Tao Hong Si Wu Tang in the treatment of lumbar intervertebral disc herniation. *World Chin Med*. 2022;17(01):37–42.
47. S K, Le P, L ZB. Effect of Right Angelica Pill on the viability of degenerated myeloid cells and expression of related inflammatory factors in liver and kidney deficiency type. *Chin J Trad Chin Med Orthop*. 2021;29(07):12–16.